

Reversal Trend of Hounsfield Unit Values of Substances with High and Low Effective Atomic Numbers

Fariba Zarei¹, Sabysachi Chatterjee², Vani Vardhan Chatterjee³, Rezvan Ravanfar Haghighi^{1,4*}

1. Medical Imaging Research Center, Shiraz University of Medical Sciences, Shiraz, Iran
2. Ongil, 79 D3, Sivaya Nagar, Reddiyur Alagapuram, Salem 636004, India
3. Department of Instrumentation and Applied Physics, Indian Institute of Science, Bangalore 560012, India
4. Nuclear Medicine and Molecular Imaging Research Center, Shiraz University of Medical Sciences, Shiraz, Iran

ARTICLE INFO

ABSTRACT

Article type:

Original Article

Article history:

Received: Aug 29, 2019

Accepted: Dec 12, 2019

Keywords:

Atomic Number

Dual-Energy

Computed Tomography

Effective Energy

Hounsfield Unit

Introduction: In dual-energy computed tomography (DECT), the Hounsfield values of a substance measured at two different energies are the basic data for finding the chemical properties of a substance. The trends of Hounsfield unit (HU) alterations following the changes in energy are different between the materials with high and low Z_{eff} . The present study aimed to analyze the basic principles related to the attenuation coefficient of x-ray photons and a quantitative explanation is given for the mentioned behavior or trend.

Material and Methods: A mathematical expression was derived for the HU difference between two different scanner voltages. Attenuation coefficients of diverse substances, such as methanol, glycerol, acetic acid, the aqueous solution of potassium hydroxide, and water were calculated for x-ray scanners operating differently at distinct applied voltages and with diverse inherent or added filters.

Results: Findings of the current study demonstrated that the negative or positive outcome of $HU(V_1) - HU(V_2)$ equation is not determined by the electron density of a substance. However, it is affected by the effective atomic number (Z_{eff}) of the material and machine parameters specified by the source spectrum.

Conclusion: According to our results, the sign of HU difference [$HU(V_1) - HU(V_2)$] for the variable cases of V_2 and V_1 gives an indication of the effective atomic number of the material under study. The obtained results might be of diagnostic value in the DECT technique.

► Please cite this article as:

Zarei F, Chatterjee S, Vardhan Chatterjee V, Ravanfar Haghighi R. Reversal Trend of Hounsfield Unit Values of Substances with High and Low Effective Atomic Numbers. Iran J Med Phys 2020; 17: 340-349. 10.22038/ijmp.2019.42841.1642.

Introduction

It is very difficult to distinguish between materials with highly similar chemical characteristics, including effective atomic number (Z_{eff}) and electron density (ρ_e) by conventional computed tomography (CT) because of their very close attenuation coefficients and HU values. The attenuation coefficient is strongly dependent on effective energy or source spectrum. Dual-energy CT (DECT) method scans the same object with two different photon energies providing two independent data that determine two distinct quantities of ρ_e and Z_{eff} for the material. Therefore, the DECT technique can discriminate between the different types of materials based on ρ_e and Z_{eff} [1-4].

The attenuation coefficient of x-ray photons in diagnostic radiology is defined as the sum of contributions from the Compton scattering and photoelectric effect. The coherent scattering is negligible due to the low-energy x-rays being eliminated from the source spectrum by different filters [5,6]. The x-ray photons that penetrate the material being studied and reach CT detectors carry attenuation coefficient data from each voxel of the material.

The CT machine is calibrated on the basis of the water attenuation coefficient as the major component in the diverse parts of the human body. The Hounsfield unit (HU) value gives a "numerical measure" of the attenuation coefficient of the material in relation to water and appears as grayscale in the CT image. At the same time, the HU value of the scanned material can be calculated using the attenuation coefficient of the material and water in case the source spectrum $S(E, V)$ and the detector efficiency $D(E)$ are known [7, 8].

Due to the polychromatic nature of the x-ray source spectrum, HU value as the output of the CT machine is related to the mean attenuation coefficient of x-ray photons taken over the source spectrum. The latter point depends on the physical characteristics of a CT machine, such as the type and thickness of the filter and voltage applied to the x-ray tube. Consequently, we require knowledge regarding the x-ray source spectrum to calculate the mean attenuation coefficient [9].

This makes the HU value of any material strongly dependent on the effective energy or source spectrum.

*Corresponding Author: Tel: + 98 7136281464; Fax: +98 7136281506; E-mail: sravanfarr@gmail.com

It has been observed that HU value in bone decreases with an increase in the effective energy of a photon, while the HU value of fat augments with an elevation in the effective energy or applied voltage [10, 11].

To the best of our knowledge, there is no physical explanation in the literature about the abovementioned changes of the HU value of substances in real quantifiable terms. With this background in mind, the current study aimed to explore a satisfactory theoretical explanation for the relationship between HU values, different voltages, machine characteristics, and material properties.

Materials and Methods

The mean attenuation coefficient of x-ray photons from the x-ray tube of the CT machine is calculated by the well-known following formula:

$$\hat{\mu}(V) = \rho_e \left[\alpha_0 \hat{f}_{KN}(V) + \beta_0 \hat{f}_{ph}(V) Z_{eff}^x \right] \quad (1)$$

where $\hat{f}_{KN}(V)$ and $\hat{f}_{ph}(V)$ are the means of the source spectrum of Compton scattering (Klein-Nishina) and photoelectric absorption, respectively. In addition, Z_{eff} refers to effective atomic number, ρ_e represents the electron density of the material, and x is the exponent of photoelectric effect [12]. The constants of $\alpha_0 = (8\pi/3)r_e^2 = 66.62 \times 10^{-26} \text{ cm}^2$ and $\beta_0 = (256\pi/3)(1/137)a_0^2 = 54.75 \times 10^{-18} \text{ cm}^2$ are the typical cross-sections for Compton scattering and photoelectric effect, respectively. In the latter formulas, $r_e = 2.82 \times 10^{-13} \text{ cm}$ is the classical radius of the electron and $a_0 = 5.29 \times 10^{-9} \text{ cm}$ is the Bohr radius of hydrogen in its ground state.

The x-ray attenuation coefficient of all substances, including water, declines with an increase in energy. The mean attenuation coefficient of the substance [$\hat{\mu}(V)$] and water [$\hat{\mu}_w(V)$] are used to calculate the HU (V) values by the following formula:

$$HU(V) = \left(\frac{\hat{\mu}(V) - \hat{\mu}_w(V)}{\hat{\mu}_w(V)} \right) \times 1000 \quad (2)$$

where the means, as indicated by the “hat” on top of the variables, are calculated over the source spectrum. The mean attenuation coefficient of the scanned material can be extracted using equation (2) as follow:

$$\hat{\mu}(V) = \hat{\mu}_w(V) \left[1 + \frac{HU(V)}{1000} \right] \quad (3)$$

If we define

$$F(V) = 1 + \frac{HU(V)}{1000} = \frac{\hat{\mu}(V)}{\hat{\mu}_w(V)} \quad (4)$$

We get the following ratio of

$$\frac{F(V_1)}{F(V_2)} = \left[\frac{\hat{\mu}_w(V_2)}{\hat{\mu}_w(V_1)} \right] \frac{\alpha_0 \hat{f}_{KN}(V_1) + \beta_0 \hat{f}_{ph}(V_1) Z_{eff}^x}{\alpha_0 \hat{f}_{KN}(V_2) + \beta_0 \hat{f}_{ph}(V_2) Z_{eff}^x} = \frac{1+HU(V_1)/1000}{1+HU(V_2)/1000} \quad (5)$$

It can be easily seen in equation (5) that for $HU(V_1) > HU(V_2)$, we need to have $[F(V_1)/F(V_2)] > 1$. Moreover, for $HU(V_1) < HU(V_2)$ we have to satisfy $[F(V_1)/F(V_2)] < 1$. As a result, to have

$\frac{F(V_1)}{F(V_2)} \geq 1$ or $F(V_1) \geq F(V_2)$, it is clear from equations (1), (4), and (5) that we should have

$$\left[\frac{\hat{\mu}_w(V_2)}{\hat{\mu}_w(V_1)} \right] \frac{\alpha_0 \hat{f}_{KN}(V_1) + \beta_0 \hat{f}_{ph}(V_1) Z_{eff}^x}{\alpha_0 \hat{f}_{KN}(V_2) + \beta_0 \hat{f}_{ph}(V_2) Z_{eff}^x} \geq 1 \quad (6)$$

In the mentioned formula, α_0 and β_0 are equal to 66.62×10^{-26} and $54.75 \times 10^{-18} \text{ cm}^2$, respectively. It could be seen that this ratio is independent of ρ_e , while it depends on Z_{eff} , as well as the machine parameters $\hat{\mu}_w(V_1), \hat{\mu}_w(V_2), \hat{f}_{KN}(V_1), \hat{f}_{KN}(V_2), \hat{f}_{ph}(V_1), \hat{f}_{ph}(V_2)$.

Finally, it could be found from equation (6) that for the cases with $HU(V_1) \geq HU(V_2)$, the Z_{eff}^x has to follow

$$Z_{eff}^x \geq 1.2168 \times 10^{-8} \left[\frac{\hat{\mu}_w(V_1) \hat{f}_{KN}(V_2) - \hat{\mu}_w(V_2) \hat{f}_{KN}(V_1)}{\hat{\mu}_w(V_2) \hat{f}_{ph}(V_1) - \hat{\mu}_w(V_1) \hat{f}_{ph}(V_2)} \right] = Z_c^x \quad (7)$$

where we have put the numerical value of $(\alpha_0/\beta_0) = 1.2168 \times 10^{-8}$ as the pre-factor in equation (7). It is important to note that this condition does not depend on electron density.

Calculation of $HU(V_1)$ - $HU(V_2)$

From the definitions, as could be observed in equation (5), it is easy to see that the difference in HU values is given by

$$[HU(V_1) - HU(V_2)] = [1000 \times F(V_2)] \times \left[\frac{F(V_1)}{F(V_2)} - 1 \right] \quad (8)$$

Using equations (5) and (7) in equation (8), we have

$$[HU(V_1) - HU(V_2)] = [1000 \times F(V_2)] \times \beta_0 Q(V_1, V_2) \times \{Z_{eff}^x - Z_c^x\} \quad (9)$$

$$Q(V_1, V_2) = [\hat{\mu}_w(V_2) \cdot \hat{f}_{ph}(V_1)] - [\hat{\mu}_w(V_1) \cdot \hat{f}_{ph}(V_2)] \quad (10)$$

Equations (9) and (10) are the basic results of the study.

We note $F(V_2) > 0$. Then it follows that in order that $HU(V_1) > HU(V_2)$, one has to satisfy any one of the following conditions:

- (1) $Z_{eff}^x > Z_c^x$ and $Q(V_1, V_2) > 0$ or
- (2) $Z_{eff}^x < Z_c^x$ and $Q(V_1, V_2) < 0$.

This can manifest itself in the following ways: (a) $HU(V_1) > HU(V_2)$ for $V_1 > V_2$ in some substances and be (b) $HU(V_1) > HU(V_2)$ for $V_1 < V_2$ for some other

substances. The idea is to check how this reversal is related to Z_{eff} and whether this is explained by conditions (1) and (2) given above. This holds key to the question "why do the HU values of fats and oils increase with elevated energy, while the HU values of bones and soft tissues decrease with an augmentation in the energy of x-ray photons?" It could be observed in the abovementioned discussions that these points might be determined by the values of $\hat{\mu}_w(V), \hat{f}_{ph}(V), \hat{f}_{KN}(V), \hat{\mu}_w(V), \hat{f}_{ph}(V), \hat{f}_{KN}(V)$, which are machine-dependent quantities.

In the next part of this study, we determine the machine parameters, including $\hat{\mu}_w(V), \hat{f}_{ph}(V), \hat{f}_{KN}(V)$ using proper source spectrum with appropriate filtration. The basic approach for determining the source spectrum and machine parameters is outlined in the next section.

Source Spectrum Calculation

In order to estimate various quantities, such as Z_c and $Q(V_1, V_2)$, it is necessary to know the values of $\hat{\mu}_w(V), \hat{f}_{ph}(V), \hat{f}_{KN}(V)$ calculated from the source spectrum $S(E, V)$. We write the source spectrum as

$$S(E, V) = S_0(E, V) \exp[-\chi(E)] \quad (11)$$

where $S_0(E, V)$ is the bare source spectrum of x-ray photons given out by the x-ray tube and $\exp[-\chi(E)]$ represents the attenuation factor due to external filtering. Moreover,

$$\chi(E) = \sum \mu_i(E) \cdot l_i \quad (12)$$

where i designates the label for a certain kind of filtering material with the thickness of l_i and attenuation coefficient of $\mu_i(E)$. The value of $\mu_i(E)$ can be estimated by equation (1) or be obtained from the NIST tables [13].

The different means can be calculated as follow:

$$\hat{f}_{KN}(V) = \int f_{KN}(E) \cdot S(E, V) dE \quad (13)$$

$$\hat{f}_{ph}(V) = \int f_{ph}(E) \cdot S(E, V) dE \quad (14)$$

$$\hat{\mu}_w(V) = \int \mu_w(V) \cdot S(E, V) dE \quad (15)$$

Experiment Procedure

We measured the HU values of pure methanol, pure acetic acid, pure glycerol, and the 30% weight/weight (w/w) solution of potassium hydroxide (KOH) in water to corroborate the mentioned explanation with observations. The Z_{eff} of the first three materials is lower than water, while the KOH solution is known as a material with high Z_{eff} . The chemicals were of analytical grade from Merck Chemicals, Germany and the samples

were prepared and studied at $22 \pm 0.5^\circ C$ as the temperature at which the CT room is maintained.

For weighting the samples, we used the MXX-123 Digital balance (Denver Instrument, Göttingen, Germany) with an accuracy of 0.01 mg and solution temperature was measured by Nuclear Associates 07-402 digital thermometer (Hicksville, New York, USA). The density of the samples was examined through the standard method using specific gravity bottles. The density was found to be within 1% of the values given as standard in the literature [14].

Although the electron density and density of the substance did not appear in equation (7), we measured density to check the accuracy of our sample preparation. These procedures have been explained in detail previously [12]. Briefly, the samples were introduced into the phantom as previously described [12] and were scanned at 80, 100, 120, 140 kVp. The DSCT SOMATOM Definition Syngo CT 2008 (Siemens, Munich, Germany) was used to scan the samples. The filter used in this DSCT machine, as noted in its manual, is equivalent to 12.8 mm aluminum (Al) and contains 7.3 mm Al+0.6 mm titanium (Ti) (0.6 mm Ti is equal to 5.5 mm Al). A typical CT image of the samples was presented in the previous studies [12].

The electron density (ρ_e) and effective atomic number of the samples were calculated using equations (7) and (10) as explained previously [12]. The equations are as follow:

$$\rho_e = \frac{\rho}{m_p} \frac{\sum_j \sum_i c(j) n(j, i) Z_i}{\sum_j \sum_i c(j) n(j, i) A_i} \quad (16)$$

$$Z_{eff}^x = \frac{\sum_j c(j) \sum_i n(j, i) Z_i^{x(i)+1}}{\sum_j c(j) \sum_i n(j, i) Z_i} \quad (17)$$

where Z_i is the atomic number and A_i is the atomic weight of the i th atom. It is clear that $w(j)$ is the w/w concentration of the j th component and we have $c(j)=w(j)/M(j)$; where $M(j)$ is the molecular weight of the j th component.

Results

For the calculation of the source spectra we followed the following steps. Firstly the Boone-Seibert formula was used to determine the bare source spectra $S_0(E, V)$ which appears in Eq. (11). Next, the factor $\exp[-\chi(E)]$ is computed by considering different types of filters. In this way the source spectra $S(E, V)$ are computed as explained in the following sentences [15].

The specification of the manufacturer is an Al filter with $l_{Al} = 7.3$ mm in combination with a Ti filter with $l_{Ti} = 0.6$ mm, the latter being equal to an Al filter of 5.5 mm thickness. This composite filter is comparable to an Al filter with a thickness of 12.8 mm. In Figure (1), we compare the source spectra in the two cases and find their shapes to be qualitatively similar. In Figure (2), the source spectrum for filtering by a filter of $l_{Al} = 12.8$ mm and an additional tin filter of $l_{Sn} = 1$ mm is presented.

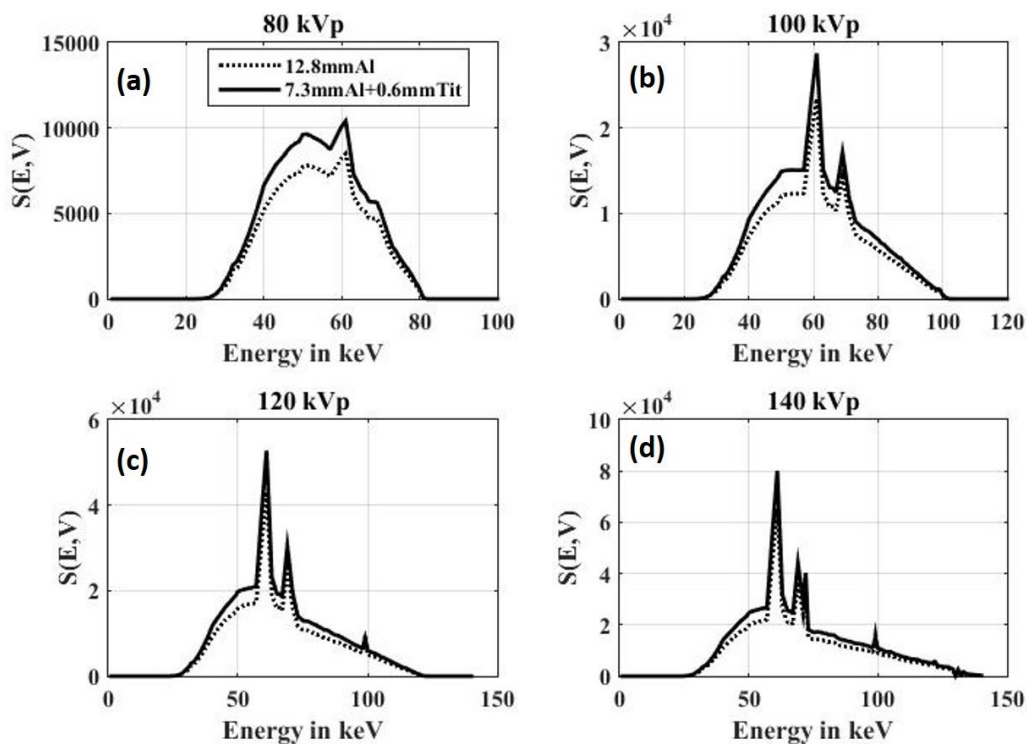


Figure 1. Variation of the source spectrum versus the energy of x-ray photons at (a) 80 kVp, (b) 100 kVp, (c) 120 kVp, and (d) 140 kVp for the two types of filtering, including (i) 12.8 mm Al and (ii) 7.3 mm Al+0.6 mm Ti filter combination in the path of the “bare” Boone-Seibert source spectrum

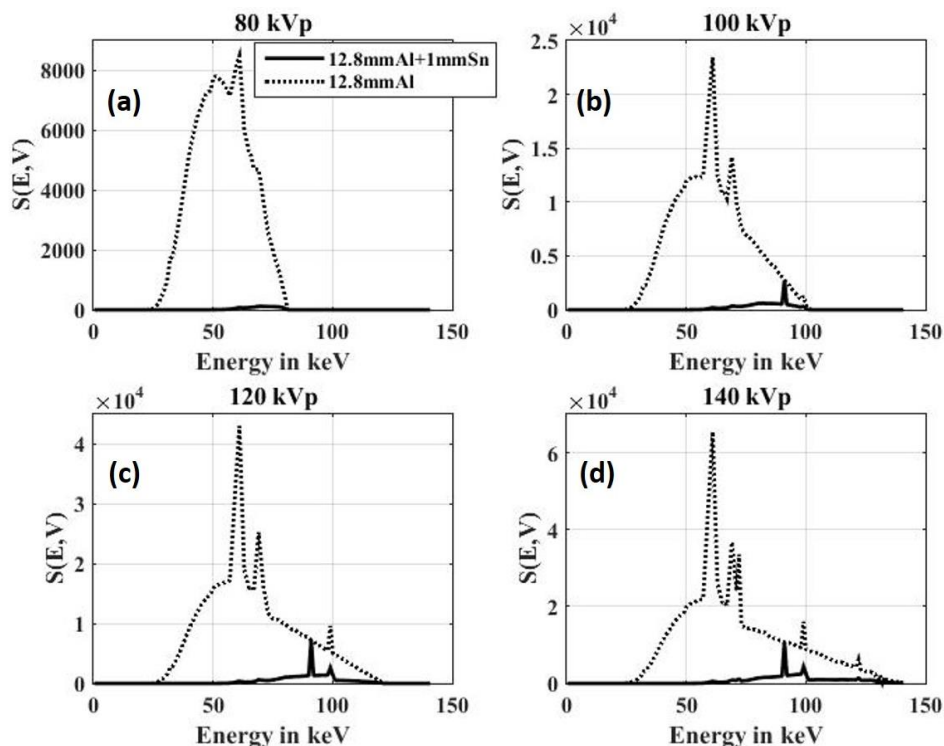


Figure 2. Variation of the source spectrum versus the energy of x-ray photons at (a) 80 kVp, (b) 100 kVp, (c) 120 kVp, and (d) 140 kVp for the two types of filtering, including (i) 12.8 mm Al and (ii) 12.8 mm Al+1 mm Sn filter combination in the path of the “bare” Boone-Seibert source spectrum

Table 1. Mean energy (\hat{E}) and standard deviation (SD) of energy for the three cases of (a) 12.8 mm Al, (b) 7.3 mm Al+0.6 mm Ti, and (c) 12.8 mm Al+1 mm Sn filters

kVp	12.8 mm Al		7.3 mm Al+0.6 mm Ti		12.8 mm Al+1 mm Sn	
	\hat{E}	SD	\hat{E}	SD	\hat{E}	SD
80	54	27	54	27	69	37
100	61	31	61	31	83	43
120	66	35	66	35	89	45
140	70	40	70	40	96	48

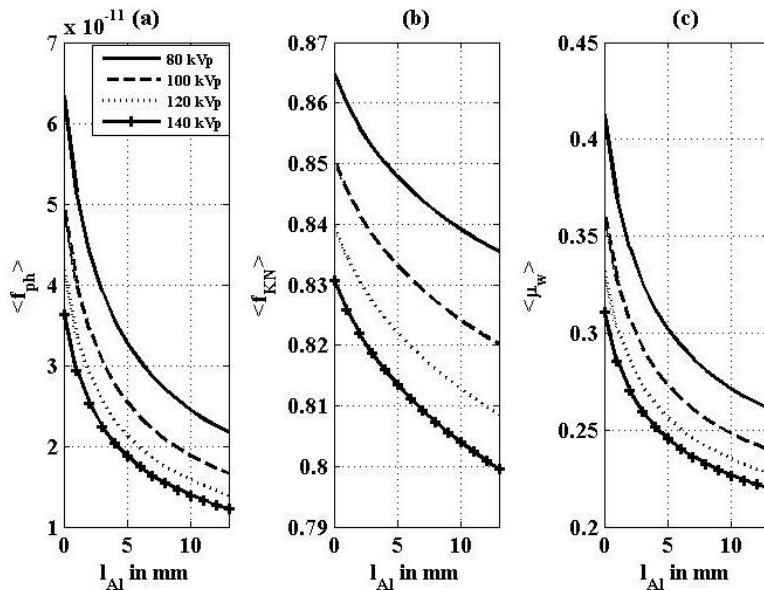


Figure 3. Variation of (a) $\hat{f}_{ph}(V)$, (b) $\hat{f}_{KN}(V)$, and (c) $\hat{\mu}_w(V)$ versus l_{Al} for $0 \leq l_{Al} \leq 13$ mm

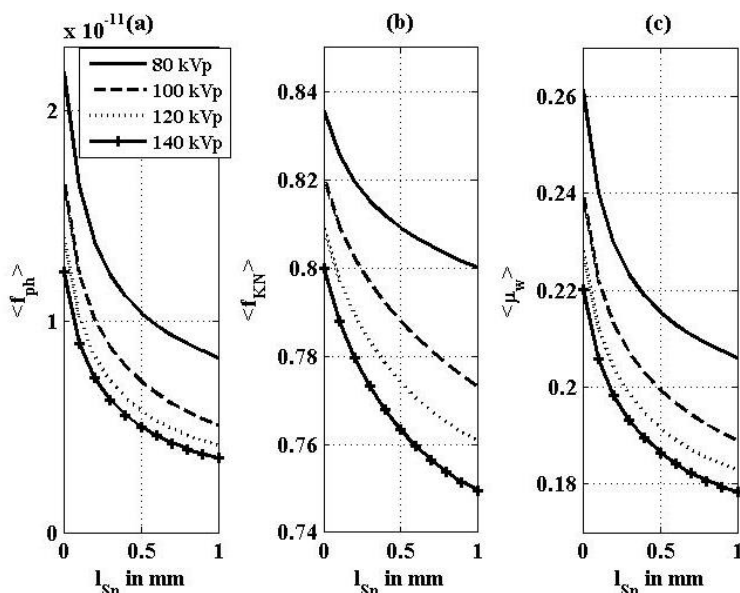


Figure 4. Mean values of photoelectric coefficient $\hat{f}_{ph}(V)$ (a), Klein-Nishina coefficient $\hat{f}_{KN}(V)$ (b), and the attenuation coefficient of water $\hat{\mu}_w(V)$ (c) at 80, 100, 120, and 140 kVp over the source spectrum when 12.8 mm Al is used in combination with the tin filter of 0-1 mm thickness

As could be seen in Table 1, the mean energy (\hat{E}) and standard deviation (SD) are the same for the composite filter of (a) $l_{Al} = 7.3 \text{ mm} + l_{Ti} = 0.6 \text{ mm}$, and (b) equivalent Al filter with $l_{Al} = 12.8 \text{ mm}$. Regarding

the case of the filter with (c) $l_{Al} = 12.8 \text{ mm} + l_{Sn} = 1 \text{ mm}$, the total number of photons was much lower. Furthermore, \hat{E} and SD were much higher than the previous two cases.

Table 2. Physical parameters $\hat{f}_{ph}(V)$, $\hat{f}_{KN}(V)$, and $\hat{\mu}_w(V)$ obtained with the filtration of Boone-Seibert spectrum using (a) $l_{Al} = 12.8$ mm and $l_{Sn} = 0$ mm, and (b) $l_{Al} = 12.8$ mm and $l_{Sn} = 1$ mm; $\hat{\mu}_w(V)$ is expressed in cm^{-1} ; this table is reproduced from the literature [6] where the method for calculating $\hat{f}_{ph}(V)$, $\hat{f}_{KN}(V)$, and $\hat{\mu}_w(V)$ is given

Energy (keV)	$\hat{f}_{ph}(V) \times 10^{-10}$		$\hat{f}_{KN}(V)$		$\hat{\mu}_w(V)$	
	(a)	(b)	(a)	(b)	(a)	(b)
80	0.2185	0.0828	0.8356	0.8	0.2613	0.206
100	0.1672	0.0508	0.8205	0.7731	0.24	0.1889
120	0.14	0.0414	0.8088	0.7608	0.228	0.1829
140	0.1235	0.0356	0.7999	0.7496	0.2202	0.1784

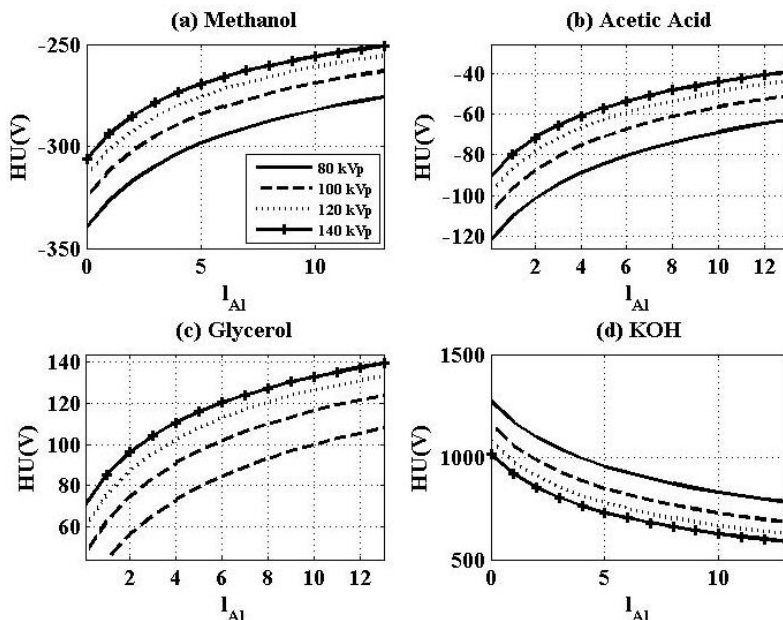


Figure 5. Variation of HU values versus the different thicknesses of Al filter (0-13 mm) at 80, 100, 120, and 140 kVp for (a) methanol, (b) acetic acid, (c) glycerol, and (d) potassium hydroxide (KOH)

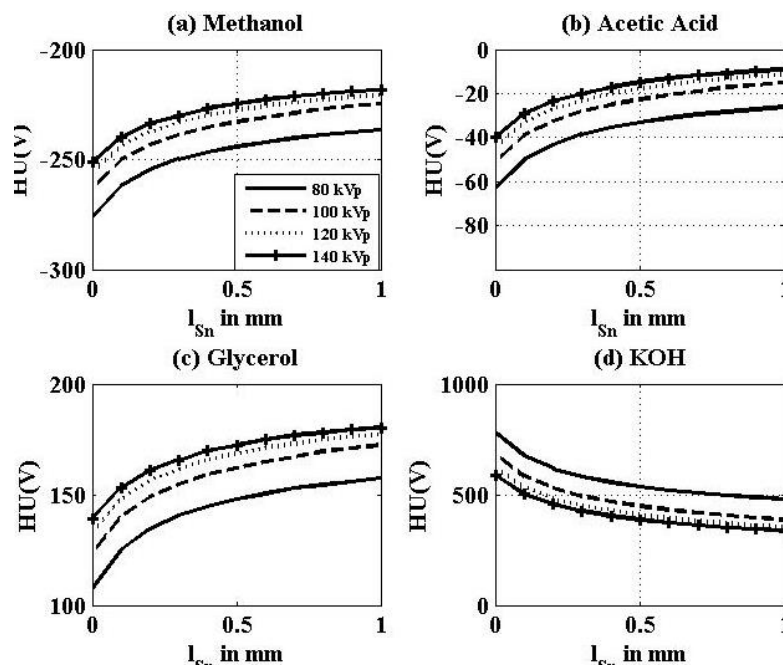


Figure 6. Variation of HU values of (a) methanol (b) acetic acid (c) glycerol, and (d) potassium hydroxide (KOH) versus the different thicknesses of tin ($0 \leq l_{Sn} \leq 1$ mm) in addition to 12.8 mm Al as the added filter to the bare Boone Seibert source spectrum

Table 3. Attenuation coefficient $\hat{\mu}(V)(\text{cm}^{-1})$ and HU(V) obtained for different source spectra applying (i) $l_{Al} = 12.8 \text{ mm}$ and $l_{Sn} = 0 \text{ mm}$ and (ii) $l_{Al} = 12.8 \text{ mm}$ and $l_{Sn} = 1 \text{ mm}$; the HU values for case (i) and (ii) are denoted by HU(Cal₁) and HU(Cal₂), respectively; the calculated $\hat{\mu}(V)$ values are obtained by $\hat{f}_{KN}(V), \hat{f}_{ph}(V)$ as presented in Table 2; the experimental $\hat{\mu}(V)$ is calculated from equation (3) in which $\hat{\mu}_w(V)$ is taken from Table 2

Substance	$\rho_e \times 10^{23}$ (cm^{-3})	Z_{eff}^x	kVp	HU(V)			$\hat{\mu}(V)$		
				Cal ₁	Cal ₂	Exp	Cal ₁	Cal ₂	Exp
Methanol	2.6577	129.5	80	-276	-237	-235	0.1891	0.1572	0.1576
			100	-263	-225	-223	0.1768	0.1465	0.1468
			120	-256	-221	-216	0.1696	0.1425	0.1434
			140	-251	-218	-214	0.1649	0.1394	0.1402
Acid Acetic	3.3493	145.5	80	-63	-26	-19	0.2448	0.2006	0.2021
			100	-51	-15	-15	0.2277	0.1861	0.1861
			120	-45	-11	-11	0.2178	0.1808	0.1809
			140	-40	-9	-8	0.2114	0.1768	0.177
Glycerol	3.3981	139.7	80	108	157	176	0.2894	0.2384	0.2423
			100	124	172	178	0.2697	0.2215	0.2225
			120	133	177	181	0.2582	0.2153	0.216
			140	139	180	184	0.2508	0.2105	0.2112
Potassium Hydroxide solution***	3.9794	592	80	781	478	684	0.4654	0.3045	0.3469
			100	684	385	547	0.4042	0.2616	0.2922
			120	626	355	478	0.3707	0.2479	0.2703
			140	589	337	434	0.3499	0.2384	0.2558

Utilizing these parameters for the different cases of l_{Ab} we first calculated the source spectrum $S(E, V)$ and then $\hat{f}_{ph}(V)$, $\hat{f}_{KN}(V)$, and $\hat{\mu}_w(V)$ for different filters. The results are shown in figures (3) and (4) and are summarized in Table 2. Afterwards, we calculated $\hat{\mu}(V)$ and HU(V) values for pure methanol, glycerol, acetic acid, and the 30% w/w solution of KOH in water as demonstrated in figures (5) and (6) and Table 3. It was revealed that in the case of high effective atomic number (Z_{eff}), such as KOH, the HU(V) reduces with a rise in voltage (kVp). On the other hand, for the cases with low Z_{eff} , including methanol, acetic acid, and glycerol, the trend is reversed and the calculated HU(V) augments with increased voltage.

It could be observed in figures (4) and (6) that for the materials with low Z_{eff} , namely methanol, acetic acid, and glycerol, we have $HU(V_1) < HU(V_2)$ when $V_1 < V_2$. However, for the materials with high Z_{eff} , such as KOH solution, we have $HU(V_1) > HU(V_2)$ when $V_1 < V_2$. Using the values of $\hat{f}_{ph}(V), \hat{f}_{KN}(V), \hat{\mu}_w(V)$ as indicated in Table 2, for $l_{Al} = 12.8 \text{ mm}$ we found $Z_c^x = 190.87$ and $Z_c = (190.87)^{1/2.55} = 7.84$ considering $x=2.55$ [16].

Regarding the Al filter with 12.8 mm thickness (i.e., case a), we designated the HU values as HU(Cal₁). The HU(Cal₁) values, as shown in Table 3, are very different from the experimental ones, which are represented by HU(Exp). The latter point leads us to believe that the equivalent filter of 12.8 mm Al, mentioned in the manual booklet, is not sufficient for removing the low-energy part of the source spectrum. Consequently, it is possible that another filter with a high Z_{eff} exists in the path of the x-ray beam to cut a larger proportion of the low-energy part of x-ray photons.

It is known that the tin (Sn) filter is often used in the newer versions of DSCT (e.g., Flash Siemens) machines in front of the source of x-ray. As a result, we assume that the materials with high Z_{eff} , such as tin (or an equivalent) may be present in the x-ray tube to cut the low part of x-ray photons for all excitation voltages.

Figure 5 (a-d) represents the corresponding HU(V) values for our different substances under study when the case is realized in practice. It could be seen that in case (1) we have $HU(V_1) < HU(V_2)$ for materials such as methanol, acetic acid and glycerol when the filtering used $l_{Al}=12.8 \text{ mm}$ and $0 \leq l_{Sn} \leq 1 \text{ mm}$. This corresponds to the case (1) given in section 2.1 of the paper. These are substances with low Z_{eff} as required in case (1). On the other hand for high Z_{eff} substances including KOH solutions we found $HU(V_1) > HU(V_2)$ for $V_1 < V_2$. This, as given in section 2.1 corresponds to case (2). This way the reversal in the trend of the HU values is given theoretical justification.

We found that our observed HU(V) values for all the four abovementioned samples, namely methanol, glycerol, and acetic acid all in the pure form and 30% w/w KOH solution in water had the best fit with the theoretical ones when we chose $l_{Al} = 12.8 \text{ mm}$ and $l_{Sn} = 1 \text{ mm}$, especially for the low- Z_{eff} solutions in which we are interested and we designated this case as case (2). The corresponding values of the machine parameters in this particular case ($l_{Al} = 12.8 \text{ mm}$ and $l_{Sn} = 1 \text{ mm}$) are given in Table 2 and the respective ρ_e and Z_{eff}^x values of the samples are presented in Table 3. The HU values for $l_{Al} = 12.8 \text{ mm}$ and $l_{Sn} = 1 \text{ mm}$ are demonstrated in Table 3.

Therefore, it is clear that in the case of $l_{Al} = 0-13 \text{ mm}$ and with a combination of 12.8 mm Al and 1 mm tin,

$HU(V_1) > HU(V_2)$ if $V_1 < V_2$ for the cases with high Z_{eff} , such as the solution of 30% w/w of KOH in water. On the other hand, for the low- Z_{eff} materials, namely methanol, acetic acid, and glycerol, we have $HU(V_1) < HU(V_2)$ for $V_1 < V_2$. The reason for the latter reversal is explained by the condition given in equations (7)-(10). This condition is independent of ρ_e but depends on the values of $\hat{f}_{ph}(V)$, $\hat{f}_{KN}(V)$, and $\hat{\mu}_w(V)$ subsequently on the source spectrum. Therefore, it is assumed to depend on the filtration superposed on the bare Boone-Seibert spectrum.

To check the matching status with the experimental data, we consider the case where the filtration is performed with $l_{Al} = 12.8 \text{ mm}$, as specified by the manufacturer. Based on the calculated values of $\hat{f}_{ph}(V)$, $\hat{f}_{KN}(V)$, and $\hat{\mu}_w(V)$ we have calculated $\hat{\mu}(V)$ and $HU(V)$ of the diverse materials. As shown in Table 3, the calculated $HU(V)$ values differ by about -40 for the low- Z_{eff} materials and their calculated $\hat{\mu}(V)$ values have a 15%-25% discrepancy. In addition to a tin filter with $l_{Sn} = 1 \text{ mm}$, the calculated $HU(V)$ values of these materials with low Z_{eff} match excellently with the observed values. However, this filtering underestimates the $\hat{\mu}(V)$ values of KOH by about 10%. The proper optimization problem will be left for future studies in the future.

Estimation of Z_c

From the calculated values of $\hat{f}_{ph}(V)$, $\hat{f}_{KN}(V)$, and $\hat{\mu}_w(V)$ we found the calculated values of Z_c^x and Z_c as follow:

Case 1: $l_{Al} = 12.8 \text{ mm}$, $l_{Sn} = 0 \text{ mm}$
 $\hat{f}_{KN}(80) = 0.8536$, $\hat{f}_{ph}(80) = 2.185 \times 10^{-11}$, $\hat{\mu}_w(80) = 0.2613$,
 $\hat{f}_{KN}(140) = 0.7999$, $\hat{f}_{ph}(140) = 1.235 \times 10^{-11}$, $\hat{\mu}_w(140) = 0.2202$,
which gives $Z_c^x = 190.87$ and $Z_c = 7.84$ applying $x = 2.55$.

Case 2: $l_{Al} = 12.8 \text{ mm}$, $l_{Sn} = 1 \text{ mm}$
 $\hat{f}_{KN}(80) = 0.8$, $\hat{f}_{ph}(80) = 8.28 \times 10^{-12}$, $\hat{\mu}_w(80) = 0.206$,
 $\hat{f}_{KN}(140) = 0.7496$, $\hat{f}_{ph}(140) = 3.56 \times 10^{-12}$, $\hat{\mu}_w(140) = 0.1784$,
which gives $Z_c^x = 191.45$ and $Z_c = 7.85$ applying $x = 2.55$.

The index x was considered as 2.55, in comparison with the NIST tables as explained in the literature [16]. Therefore, for $Z_{eff} < Z_c$ we have $HU(140) > HU(80)$ and for $Z_{eff} > Z_c$ we have $HU(140) < HU(80)$ and this condition has no dependence on the electron density ρ_e . Furthermore, the value of Z_c (7.84-7.85) is very close to that of water ($Z_{eff, water} = 7.566$) for a very wide range of source spectra.

Discussion

To the best of our knowledge, the question of whether the HU values of substances increase or decrease with the changes in the voltage applied to the CT machine has not been explained on the basis of underlying physics in the existing literature [8]. It is known that the HU values of several substances, such as bone, soft tissue, contrast material, left ventricular cavity, myocardium, vertebrae, and calcified plaque diminish with an elevation in photon energy. On the other hand, many experimental investigations have reported that fats, oils, and lipid-rich plaque follow the opposite trend and their HU values augment with a rise in the voltage [10, 11, 17, 18].

It is noteworthy that the machine characteristics have never been assessed in the reports. Nonetheless, it is recognized that HU values are machine-dependent, which is very explicitly stated in the literature [16, 18, 19]. In other words, several experimental studies "revealed that for the materials with effective low atomic number, the mean CT number increased with an elevation in the energy, which was opposite of the materials with an effective high atomic number" [18]-where CT number is an alternative terminology in literature which actually means HU value. The empirical data of other authors found that for the substances with an effective atomic number lower than water, the first trend occurs, while the latter trend takes place for the substances with an effective atomic number greater than water.

The present theoretical study correctly explains this reversal and clarifies the reversal in relation to the effective atomic number of water. However, it is not possible to calculate the $[HU(V_1)-HU(V_2)]$ values by equations (9) and (10) and compare them with the values given by different authors because the source spectra in their scanners, in addition to ρ_e and Z_{eff} values of the substances, are unknown. Nevertheless, equations (9) and (10) give a basis for the phenomena observed by various authors.

We aimed to explain this behavior according to the fundamental physics behind the attenuation of x-rays in materials. Our theoretical analysis showed that the reversal in the trend of $HU(V)$ variation on V depends on the ρ_e of the material, Z_{eff}^x of the material, and the parameters $\hat{f}_{KN}(V)\hat{f}_{ph}(V)$ of the CT machine. Applying this physical analysis, we are able to identify $Z_{eff}^x = Z_c^x$ at which the trend actually alters. For $Z_{eff}^x \geq Z_c^x$, HU declines with an increase in kVp , while for $Z_{eff}^x \leq Z_c^x$, HU value elevates with an augmentation in kVp .

In terms of machine parameters, the numerical value of Z_c^x can be calculated as given in equation (7) and it was found that $Z_c \approx Z_{eff, water}$. The significance of machine parameters in determining the HU with kVp is clarified by our results in tables 2 and 3. Consequently, it is important to explore distinct methods to reliably calculate machine parameters, such as source spectrum [20] and the abovementioned findings could be accurately quantified.

It is remarkable that in spite of the significant differences between the source spectra and machine parameters [$\hat{f}_{KN}(V), \hat{f}_{ph}(V), \hat{\mu}_w(V)$] used to calculate the transition point Z_c , the actual value of Z_c may not alter much in diverse machines utilized for practical applications. It is observed that even for the cases with widely different source spectra as in (1) 12.8 mm Al+0 mm Sn and (2) 12.8 mm Al+1 mm Sn, the values of Z_c are very close to each other and can be taken as $Z_c \approx 7.85$. Then it may be possible to characterize the type of tissue using DECT scanning and checking whether $HU(V_1) < HU(V_2)$ when $V_1 < V_2$. In case the latter point is correct we can conclude that the Z_{eff} of the sample satisfies $Z_{eff} < Z_c \approx 7.85$.

This point needs to be illustrated with an example that we came across in the course of studies on non-calcified coronary artery plaque. We know that $Z_{eff}^x \leq 190.87$ for pure fats and other pure lipids (without any contamination with high-Z materials). As a result, the DSCT machine should show their HU values to increase with elevated kVp considering the parameters represented in Figure 1. This is one of the ways by which several investigators [10, 11, 19, 21] tried to identify pure fats and our method gives a physical justification for that. However, our observations with lipid plaques (composed of fats) in the coronary artery [16] do not reveal the HU values to diminish with augmented voltage. Therefore, we concluded in our earlier studies [16] that these plaques have contamination with high-Z materials.

The mentioned conclusion is justified based on the analysis presented in the current paper. Moreover, it was supported by the histopathological evidence of microcalcification in these plaques [16]. These observational details are reported in the literature [19] and further details will appear as a separate publication elsewhere. These evaluations are of clinical importance in the preliminary identification of the material forming coronary artery plaques by DECT (can tell whether $Z_{eff} < Z_c \approx 7.85$ or otherwise). Furthermore, the latter findings can in the future lead to advances in the non-invasive diagnosis of these materials and subsequently to clinical interventions in treatment.

Conclusion

Regarding the low- Z_{eff} materials, including methanol, acetic acid, and glycerol for which $Z_{eff} < Z_c$, we have $HU(V_1) < HU(V_2)$ when $V_1 < V_2$. Conversely, for cases with $Z_{eff} > Z_c$, such as KOH solution we have $HU(V_1) > HU(V_2)$ when $V_1 < V_2$. The present study demonstrates that the crossing point would take place at a Z_{eff} higher than the critical $Z_{eff} = Z_c \approx Z_{eff, water}$. In addition, the value of critical effective atomic number or Z_c depends on effective energy (source spectrum), while it has no dependence on ρ_e . This finding can be useful in the application of CT scan with two different energies, which is known as the DECT method.

Acknowledgment

The authors of this study would like to acknowledge the reviewers for their concerns that improved the manuscript and many sections were added and rewritten.

References

1. Rutherford RA, Pullan BR, Isherwood I. Measurement of effective atomic number and electron density using an EMI scanner. *Neuroradiology*. 1976;11(1): 15-21.
2. Heismann BJ, Leppert J, Stierstorfer K. Density and atomic number measurements with spectral x-ray attenuation method. *J. Appl. Phys.* 2003; 94(3): 2073-9.
3. Bazalova M, Carrier JF, Beaulieu L Verhaegen F. Dual-energy CT-based material extraction for tissue segmentation in Monte Carlo dose calculations. *Phys. Med. Biol.* 2008; 53(9): 2439-56.
4. Alvarez RE, Macovski A. Energy selective reconstruction in x-ray computerized tomography. *Phys. Med. Biol.* 1976; 21(5): 733-44.
5. Heismann BJ, Balda B. Quantitative image-based spectral reconstruction for computed tomography. *Med. Phys.* 2009; 36(10): 4471-85.
6. Haghghi RR, Chatterjee S, Kumar P, Vani VC. Numerical analysis of the relationship between the photoelectric effect and Energy of the x-ray photons in CT. *Front. Bio. Tech.* 2014 1(4): 240-51.
7. Seeram E. *Computed Tomography, Physical Principles, Clinical Applications, Quality Control*. W.B. Saunders Co. Philadelphia, 2001.
8. Zata LM, Alvarez RE. An inaccuracy in computed tomography: The energy dependence of CT values. *Radiology*. 1977; 124(1): 91-7.
9. Ay MR, Shahriyari M, Sarkar S, Adib M, Zaidi H. Monte Carlo simulation of x-ray spectra in diagnostic radiology and mammography using MCNP4C. *Phys. Med. Biol.* 2004; 49(21), 4897-917.
10. Okayama S, Soeda T, Takami Y, Kawakami R, Somekawa S, Uemura S, et al. The influence of effective energy on computed tomography number depends on tissue characteristics in monoenergetic cardiac imaging. *Radiology research and practice*. 2012;2012.
11. Raptopoulos V, Karella A, Bernstein J, Reale FR, Constantinou C, Zawacki JK. Value of dual-energy CT in differentiating focal fatty infiltration of the liver from low-density masses. *AJR*. 1991; 157(4): 721-25.
12. Haghghi RR, Chatterjee S, Vyas A, Kumar P, Thulkar S. X-ray Attenuation Coefficient of Mixtures: Inputs for Dual-Energy CT. *Med. Phys.* 2011; 38(10): 5270-9.
13. Hubbell JH, Seltzer SM. Table of x-ray mass attenuation coefficients from 1 keV to 20 MeV for elements Z ¼ 1-92 and 48 additional substances of dosimetric interest. Available URL:<http://physics.nist.gov/PhysRefData/Xcom/htm/l/xcom1.html>.
14. Sunga R. *Handymath.com Solutions for Technicians*. Available From: <http://www.handymath.com/mission.html>.
15. Boone JM, Seibert JA. An accurate method for computer-generating tungsten anode x-ray spectra

- from 30 to 140 kV. *Med. Phys.* 1997; 24(11): 1661-70.
- 16. Haghghi RR. Evaluation of coronary artery plaque. Thesis submitted to the faculty of All India Institute of Medical Sciences, New Delhi for the degree of Doctor of Philosophy, Medical Physics Unit, Dr. B. R. A. Institute Rotary Cancer Hospital, All India Institute of Medical Sciences, New Delhi-110029. 2013.
 - 17. Johnson TRC, Krauß B, Sedlmair M, Grasruck M, Bruder H, Morhard D, et al. Material differentiation by dual energy CT: initial experience. *Eur Radiol.* 2007; 17: 1510-7.
 - 18. Mahmoudi R, Jabbari N, Aghdasi M, Khalkhali HR. Energy dependence of measured CT numbers on substituted materials used for CT number calibration of radiotherapy treatment planning systems. *PLoS ONE.* 2016; 11(7): e0158828.
 - 19. Haghghi RR, Chatterjee S, Tabin M, Sharma S, Jagia P, Ray R, et al. DECT evaluation of non-calcified coronary artery plaque. *Med. Phys.* 2015; 42(10): 5945-54.
 - 20. Sidky EY, Yu L, Pan X, Zou Y, Vannier M. A robust method of x-ray source spectrum estimation from transmission measurements: Demonstrated on computer simulated, scatter free transmission data. *J. Appl. Phys.* 2005; 97(12): 124701-11.
 - 21. Halvorsen RA, Korobkin M, Ram PC, Thompson WM. CT appearance of focal fatty infiltration of the liver. *American Journal of Roentgenology.* 1982;139(2):277-81.